Tetraether Bolaform Amphiphiles as Models of Archaebacterial Membrane Lipids: Raman Spectroscopy, ^{31}P NMR, X-ray Scattering, and Electron Microscopy

David H. Thompson,*,† Kim F. Wong,‡ Robin Humphry-Baker,§ Jeffery J. Wheeler,‡ Jong-Mok Kim,† and Shankar B. Rananavare†

Contribution from the Biomolecular Materials Research Group, Department of Chemical and Biological Sciences, Oregon Graduate Institute of Science & Technology, 19600 N.W. von Neumann Drive, Beaverton, Oregon 97006-1999, Department of Biochemistry, University of British Columbia, Vancouver, British Columbia V6T 1Z3, Canada, and Institut de Chimie Physique, Ecole Polytechnique Federale de Lausanne, CH-1015 Ecublens, Lausanne, Switzerland.
Received April 13, 1992

Abstract: Freeze-fracture and cryo-transmission electron microscopy, low-angle X-ray scattering, ^{31}P NMR, and Raman spectroscopy have been used to characterize the properties of synthetic tetraether bolaform amphiphiles in aqueous solution (Kim, J.-M.; Thompson, D. H. *Langmuir* **1992**, *8*, 637-644). A mixture of morphologies composed of multilamellar vesicles, quasioriented multilamellar stacks, and isolated lamellar sheets, observed by electron microscopy immediately after sonication of 1,1′-*O*-eicosamethylene-2,2′-di-*O*-decyl-*rac*-diglycero-3,3′-diphosphate (**1**), 1,1′-di-*O*-decyl-2,2′-*O*-eicosamethylene-3,3′-diphosphate (**2**), 1,1′-*O*-eicosamethylene-2-*O*-eicosyl-*rac*-diglycero-3,2′,3′-diphosphate (**3**), and 1,1′-*O*-hexadecylmethylene-2,2′-di-*O*-octyl-*rac*-diglycero-3,3′-diphosphate (**4**) in imidazole buffer, were converted to large unilamellar and multilamellar vesicles upon heating above T_c. Axially symmetric powder pattern lineshapes, consistent with a lamellar phase, were observed by ^{31}P NMR for the hydrated lipids **1**-**4** below T_c; an isotropic signal also appeared above T_c or upon jumping the pH to 10.0. Small-angle X-ray scattering results indicate a lamellar spacing of 35.2 Å for dry **1** below its phase transition temperature that is reduced to 27.2 Å upon passing through T_c. Raman spectra revealed a high degree of alkyl chain ordering at room temperature which gradually decreased as the solution temperature was increased. These data support a model wherein the bolaform amphiphiles span a monolayer-type membrane with both polar headgroups residing at opposing membrane interfaces and disfavor one requiring large contributions from U-shaped bolalipid configurations within the lamellar phase. These data also suggest that the lipid molecular structure and dispersion method are both important determinants of solution morphology.

Introduction

The discovery of methanogenic, halophilic, and thermacidophilic archaebacteria, which thrive in harsh physical environments that are lethal to most other organisms, has stimulated research into the unique structural, biochemical, and physical properties of their membrane lipids.[1-14] Synthetic bolaform amphiphiles,[15-31] modeled after their bipolar ether lipids, are an important class of biomimetic materials that provide insight into membrane stabilization strategies that do not involve polymerization, since this approach is known to introduce structural defects within the lamellar plane.[32-36] The wide variety of bolaform materials studied so far clearly show that ultrathin membranes can be made that are stable to elevated temperatures,[22] pH extremes,[17] and high ionic strengths.[20] This stability range is appropriate for bolaamphiphile applications in cellular transfection,[18] surface derivatization,[37-41] and immobilization of integral membrane protein receptors;[42,43] however, monolayer membrane films with stabilities greater than those presently known are required for photocatalytic membranes and other composite architectures.

Our interest in bolaform lipid materials lies in their prospects for forming low-viscosity, extremely thin, durable lamellar films that are ideally suited for transmembrane electron transfer studies and photoinduced charge separation membranes.[19-22,44] The related series of lipids shown in Figure 1 were designed to probe the effects of molecular structure on their physical properties and supramolecular organization in aqueous solution. Previously reported electron micrographs of 1,1′-*O*-eicosamethylene-2,2′-di-*O*-decyl-*rac*-diglycero-3,3′-diphosphate (**1**, PS20), 1,1′-di-*O*-decyl-2,2′-*O*-eicosamethylene-3,3′-diphosphate (**2**, SS20), 1,1′-*O*-eicosamethylene-2-*O*-eicosyl-*rac*-diglycero-3,2′,3′-diphosphate (**3**, PA20), and 1,1′-*O*-hexadecamethylene-2,2′-di-*O*-octyl-*rac*-diglycero-3,3′-diphosphate (**4**, PS16), stained with phosphotungstic acid after dispersion in imidazole buffer, suggested that the bolaamphiphiles self-assembled into ~28-Å thick stacked lamellae.[22] The vulnerability of this method to stain-induced artifacts[45] led

* To whom correspondence should be addressed.
† Oregon Graduate Institute of Science & Technology.
‡ University of British Columbia.
§ Visiting Scientist, Ecole Polytechnique Federale de Lausanne.

(1) Kates, M. In *Ether Lipids: Chemistry and Biology*; Snyder, F., Ed.; Academic Press: New York, 1972; pp 351-398.
(2) Langworthy, T. A. In *The Bacteria*; Woese, C. R., Wolfe, R. S., Eds.; Academic Press: New York, 1985; Vol. 8, pp 459-491.
(3) Woese, C. R. *Microbiol. Rev.* **1987**, *51*, 221-271.
(4) De Rosa, M.; Lanzotti, V.; Nicolaus, B.: Trincone, A.; Gambacorta, A. In *Microbiology of Extreme Environments and Its Potential for Biotechnology*; DaCosta, M. S., Duarte, J. C., Williams, R. A. D., Eds.; Elsevier: New York, 1989; pp 131-151.
(5) Heathcock, C. H.; Finkelstein, B. L.; Aoki, T.; Poulter, C. D. *Science* **1985**, *229*, 862-864.
(6) Poulter, C. D.; Aoki, T.; Daniels, L. *J. Am. Chem. Soc.* **1988**, *110*, 2620-2624.
(7) Kakinuma, K.; Yamagishi, M.; Fujimoto, Y.; Ikekawa, N.; Oshima, T. *J. Am. Chem. Soc.* **1990**, *112*, 2740-2745.
(8) Nicolaus, B.; Trincone, A.; Esposito, E.; Vaccaro, M. R.; Gambacorta, A.; De Rosa, M. *Biochem. J.* **1990**, *266*, 785-791.
(9) De Rosa, M.; Gambacorta, A. *Prog. Lipid Res.* **1988**, *27*, 153-175.
(10) Gulik, A.; Luzzati, V.; De Rosa, M.; Gambacorta, M. *J. Membr. Biol.* **1985**, *182*, 131-149. Revised identifications of cubic phases have recently been made: Luzzati, V.; Vargas, R.; Gulik, A.; Mariani, P.; Seddon, J. M.; Rivas, E. *Biochemistry* **1992**, *31*, 279-285.
(11) Quinn, P. J.; Kates, M.; Tocanne, J.-F.; Tomoaia-Cotisel, M. *Biochem. J.* **1989**, *261*, 377-81.
(12) Rolandi, R.; Schindler, H.; De Rosa, M.; Gambacorta, A. *Eur. Biophys. J.* **1986**, *14*, 19-27.
(13) Bruno, S.; Gliozzi, A.; Cannistraro, S. *J. Phys.* **1986**, *47*, 1555-1563.
(14) Bruno, S.; Cannistraro, S.; Gliozzi, A.; De Rosa, M.; Gambacorta, A. *Eur. Biophys. J.* **1985**, *13*, 67-76.
(15) Führhop, J.-H.; Fritsch, D. *Acc. Chem. Res.* **1986**, *19*, 130-137.
(16) Führhop, J.-H.; David, H.-H.; Mathieu, J.; Liman, U.; Winter, H.-J.; Boekema, E. *J. Am. Chem. Soc.* **1986**, *108*, 1785-1791.
(17) Führhop, J.-H.; Liman, U.; Koesling, V. *J. Am. Chem. Soc.* **1988**, *110*, 6840-6845.
(18) Führhop, J.-H.; Tank, H. *Chem. Phys. Lipids* **1987**, *43*, 193-213.
(19) Führhop, J.-H.; Krull, M.; Schulz, A.; Möbius, D. *Langmuir* **1990**, *6*, 497-505.
(20) Führhop, J.-H.; Hungerbühler, H.; Siggel, U. *Langmuir* **1990**, *6*, 1295-1300.
(21) Arrhenius, T. S.; Blanchard-Desce, M.; Dvolaitzky, M.; Lehn, J.-M.; Malthete, J. *Proc. Natl. Acad. Sci. U.S.A.* **1986**, *83*, 5355-5359.

0002-7863/92/1514-9035$03.00/0

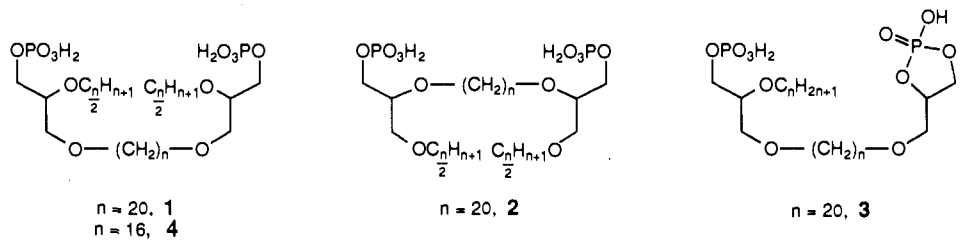

Figure 1. Structures of synthetic bolaform lipids **1–4**.

us to seek additional experimental evidence for their solution structure. A more detailed characterization of aggregate morphologies, phase behaviors, chemical resistance, and thermal stabilities of hydrated tetraethers **1–4** is described in this paper with the aim of elucidating the structure–property relationships that control stability in synthetic bipolar tetraether lipid membranes.

Experimental Methods

All bolaform lipids used in this work were determined to be pure by ^{1}H NMR and TLC and gave satisfactory analytical results.[22] Samples for physical characterization were either hydrated in pure H_2O or D_2O and equilibrated for 24+ h at room temperature or sonicated at ambient temperature in 30–40 mM imidazole buffer at pH 7 using a Heat Systems W-225 sonicator with a half-inch probe operating continuously at 30 W for 10 min unless otherwise noted.

Small-angle X-ray diffraction studies were carried out using a Phillips XRG-2500 generator operating at 35 kV and 20 mA and a sealed, fine-focus copper tube. The X-ray beam was monochromatized using a β-nickel filter and collimated using a pinhole collimator. The dry **1** lipid sample was prepared in a Mark capillary (1 mm o.d.) and placed in a temperature-regulated (±0.25 °C) chamber. The diffraction patterns were collected with a linear position sensitive detector (spatial resolution 92 μm) interfaced to a personal computer through a Nuclear Data multichannel analyzer. Sample–detector distance (12 cm) was adjusted to enable simultaneous detection of small- and wide-angle diffraction peaks.

Transmission electron microscopy (TEM) experiments were performed on hydrated and sonicated samples. Freeze-fracture and freeze-etch replicas, prepared as described by Hope et al.[46] using a Balzers BAF400D apparatus, were imaged using a JEOL JEM-1200EX microscope. Freeze-etching of the samples was used to enhance contrast in the replicas between lipid microstructures and the vitreous ice surrounding them. Direct visualization of **1** using cryo-TEM was performed using a Zeiss EM 90 electron microscope operating at 60 kV with a liquid nitrogen-cooled cryostage. Sample preparation[47–49] involved liquid propane fast-freezing and subsequent transfer to the electron microscope using a Reichert-Jung Model KF80 apparatus.

^{31}P NMR experiments of D_2O-hydrated samples, equilibrated for 12–48 h at ambient temperature with 25–55 mg of dry lipid in 2 mL of D_2O prior to analysis, were performed using a Bruker MSL 200 spectrometer and a 10-mm probe.[50,51] pH jump ^{31}P NMR experiments utilized 30 mg of dry lipid suspended in 1.5 mL of D_2O; solution pH was controlled by titration with 5 M NaOH or 6 M HCl and checked with a pH meter.

Raman spectra of hydrated samples (1 mL/5 mg of dry lipid) at pH 2.6 were collected with 150-mW excitation at 457.9 nm (1.0 cm^{-1} scan rate and 4.6 cm^{-1} slit width) using a Dilor Z 16 spectrometer interfaced to a personal computer and background-corrected by solvent subtraction as described previously.[52]

Table I. Temperature-Dependent ^{31}P NMR Chemical Shift Anisotropies

	$\Delta\sigma$ (ppm)			
T (°C)	**1**	**2**	**3**	**4**
80			33	
70			36	
65	36	18		18
60			40	
58	36	19		19
50	37	19	42	20
43	39	23		20
40			42	
35	42	31		20
30			54	
28	44	33		20
20	46	33	54	20
0	58		79	
−20	92			
−40	144		110	

Results

1. ^{31}P NMR Spectroscopy. Temperature-dependent proton-decoupled ^{31}P NMR spectra for the hydrated bipolar lipids **1–4** are shown in Figures 2A–D. Each bolaform lipid spectrum above room temperature was characterized by axially symmetric powder pattern line shapes with effective chemical shift anisotropies (CSAs) of 18–54 ppm (Table I), indicative of lamellar phase lipid. Spectra of **1–3** throughout the temperature range studied had

(22) Kim, J.-M.; Thompson, D. H. *Langmuir* **1992**, *8*, 637–644.
(23) Yamauchi, K.; Sakamoto, Y.; Moriya, A.; Yamada, K.; Hosokawa, T.; Higuchi, T.; Kinoshita, M. *J. Am. Chem. Soc.* **1990**, *112*, 3188–3191.
(24) Yamauchi, K.; Moriya, A.; Kinoshita, M. *Biochim. Biophys. Acta* **1989**, *1003*, 151–160.
(25) Bader, H.; Ringsdorf, H. *Faraday Discuss. Chem. Soc.* **1986**, *81*, 329–337.
(26) Carmichael, V. E.; Dutton, P. J.; Fyles, T. M.; James, T. D.; Swan, J. A.; Zojaji, M. *J. Am. Chem. Soc.* **1989**, *111*, 767–769.
(27) Decher, G.; Hong, J. D. *Ber. Bunsenges. Phys. Chem.* **1991**, *95*, 1430–1434.
(28) Nagawa, Y.; Regen, S. L. *J. Am. Chem. Soc.* **1991**, *113*, 7237–7240.
(29) Hentrich, F.; Tschierske, C.; Zaschke, H. *Angew. Chem., Int. Ed. Engl.* **1991**, *30*, 440–441.
(30) Dahlhoff, W. V. *Z. Naturforsch.* **1988**, *43B*, 1367–1369.
(31) Bunton, C. A.; Dorwin, E. L.; Savelli, G.; Si, V. C. *Recl. Trav. Chim. Pays-Bas* **1990**, *109*, 64–69.
(32) Lopez, E.; O'Brien, D. F.; Whitesides, T. H. *J. Am. Chem. Soc.* **1982**, *104*, 305–307.
(33) Freeman, F. J.; Hayward, J. A.; Chapman, D. *Biochim. Biophys. Acta* **1987**, *924*, 341–351.
(34) Neumann, R.; Ringsdorf, H. *J. Am. Chem. Soc.* **1986**, *108*, 487–490.
(35) Sackmann, E.; Eggl, P.; Fahn, C.; Bader, H.; Ringsdorf, H.; Schollmeier, M. *Ber. Bunsenges. Phys. Chem.* **1985**, *89*, 1198–1208.
(36) Stefely, J.; Markowitz, M. A.; Regen, S. L. *J. Am. Chem. Soc.* **1988**, *110*, 7563–7569.
(37) Whitesides, G. M.; Laibinis, P. E. *Langmuir* **1990**, *6*, 87–96.
(38) Maoz, R.; Sagiv, J. *Langmuir* **1987**, *3*, 1034–1044.
(39) Lee, H.; Kepley, L. J.; Hong, H.-G.; Mallouk, T. E. *J. Am. Chem. Soc.* **1988**, *110*, 618–620.
(40) Katz, H. E.; Scheller, G.; Putvinski, T. M.; Schilling, M. L.; Wilson, W. L.; Chidsey, C. E. D. *Science* **1991**, *254*, 1485–1487.
(41) Miller, C.; Cuendet, P.; Grätzel, M. *J. Phys. Chem.* **1991**, *95*, 877–886.
(42) Kurrle, A.; Rieber, P.; Sackmann, E. *Biochemistry* **1990**, *29*, 8274–8282.
(43) Miyasaka, T.; Koyama, K.; Itoh, I. *Science* **1992**, *255*, 342–344.
(44) Thompson, D. H.; Kim, J. M. In *Macromolecular Host-Guest Complexes: Optical, Optoelectronic, and Photorefractive Properties and Applications*; Jenekhe, S. A., Ed.; MRS Symposium Series, Vol. 277. In press.
(45) Talmon, Y. *J. Colloid Interface Sci.* **1983**, *93*, 366–382.
(46) Hope, M. J.; Wong, K. F.; Cullis, P. R. *J. Electron Microsc. Tech.* **1989**, *13*, 277–287.
(47) Bellare, J. R.; Davis, H. T.; Scriven, L. E.; Talmon, Y. *J. Electron Microsc. Tech.* **1988**, *10*, 87–111.
(48) Dubochet, J.; Adrian, M.; Chang, J.-J.; Homo, J.-C.; Lepault, J.; McDowall, A. W.; Schultz, P. *Q. Rev. Biophys.* **1988**, *21*, 129–228.
(49) Vinson, P. K.; Bellare, J. R.; Davis, H. T.; Miller, W. G.; Scriven, L. E. *J. Colloid Interface Sci.* **1991**, *142*, 74–91.
(50) Tilcock, C. P. S.; Cullis, P. R.; Hope, M. J.; Gruner, S. *Biochemistry* **1986**, *25*, 816–822.
(51) Ruocco, M. J.; Siminovitch, D. J.; Griffin, R. G. *Biochemistry* **1985**, *24*, 2406–2411.
(52) Humphry-Baker, R.; Thompson, D. H.; Lei, Y.; Hope, M. J.; Hurst, J. H. *Langmuir* **1991**, *7*, 2592–2601.

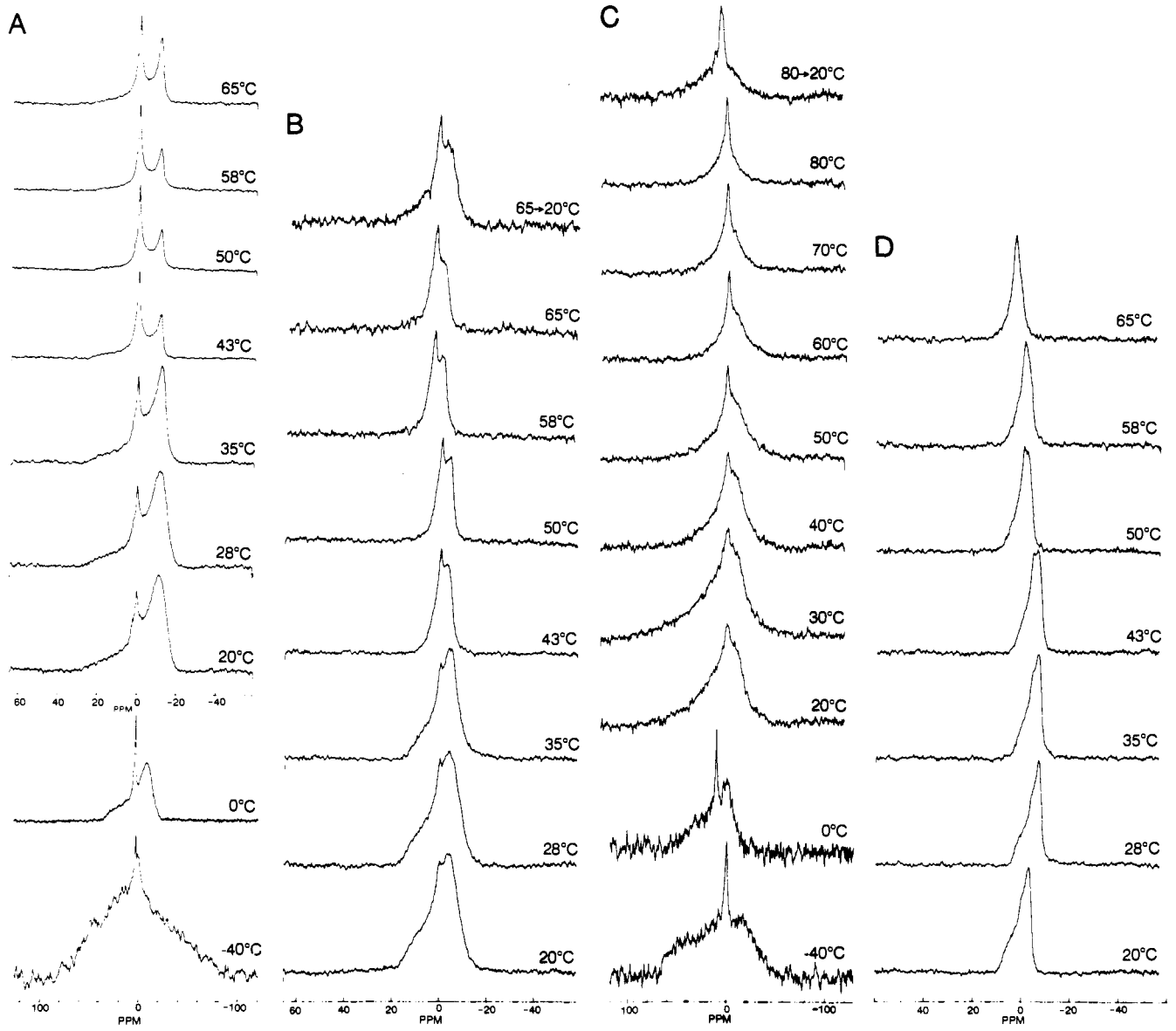

Figure 2. Temperature-dependent ^{31}P NMR of hydrated lipids **1–4**. NMR spectra were acquired using 25-W decoupling power, 49° (for **1** and **3**) or 72° (for **2** and **4**) pulses (0.1-s and 0.05-s acquisition times, respectively), and a 1-s relaxation time with 3000–24 000 scans, depending on lipid concentration, to obtain good S/N ratios.[50,51] A: **1**, 55 mg/mL. B: **2**, 40 mg/mL. C: **3**, 25 mg/mL. D: **4**, 40 mg/mL.

varying proportions of a superimposed narrow line resonance, suggesting that a fraction of the lamellar phosphorus environment was isotropic on the NMR timescale. Line shapes of **1** between 0 and 50 °C are similar to those reported for 1,2-dilauroyl-*sn*-glycero-3-phosphate[53] and the monopolar ether lipid 1,2-dihexadecyl-*sn*-glycero-3-phosphatidylcholine.[51] Upon being cooled to −40 °C, an axially asymmetric rigid lattice line shape was obtained for **3** while a broadened, motionally averaged spectrum remained for **1**. The low CSAs observed for **2** and **4** relative to **1** and **3** over the temperature range studied are consistent with other short-chain phosphate amphiphiles (e.g., lamellar sodium dibutyl phosphate mesophases reported by Chachaty and Quaegebeur[54]) having low T_cs.[22] We infer from these experiments that the liquid crystalline lamellar phases of **2** and **4** are more disordered and have higher axial rotational diffusion coefficients than those of **1** or **3** at the same temperature.

The isotropic signals superimposed on the spectra of **1**, **2**, and **3** arise from dispersion of the bolaform amphiphiles due to heating or a jump in pH. A rapid pH jump (<10 s) of hydrated **1** from pH 3.8 to 10.0 at ambient temperature[53,55] converted the axially symmetric powder pattern (Figure 3A) to an isotropic signal (Figure 3B) due to high pH-induced micelle or vesicle formation. Neutralization of the basic lipid solution retained a small fraction of the isotropic signal; however, the spectrum is predominantly an axially symmetric powder pattern line shape (compared Figures 2A and 3C). This observation is consistent with the temperature-dependent results wherein an isotropic phosphorus signal generated during a previous heating cycle persists upon cooling due to heat-induced vesicle formation (Figures 2A–C and Discussion).

2. Transmission Electron Microscopy. Negatively stained electron micrographs showing lamellar dispersions of **1–4** have been reported by our laboratory;[22] however, additional experiments were necessary to rule out the possibility of staining artifacts. Confirmation of the structural assignments made on the basis of ^{31}P-NMR results and investigation of the morphological changes that might occur as a function of sample preparation, age, co-surfactant, and elevated temperature were also of interest. These studies, using two complementary EM methods, are described below.

2.1. Freeze-Fracture TEM. The effects of sonication, aging, heating, and the addition of 1,2-dilauroyl-*sn*-glycero-3-phospho-

(53) Hauser, H.; Mantsch, H. H.; Casal, H. L. *Biochemistry* **1990**, *29*, 2321–2329.
(54) Chachaty, C.; Quaegebeur, J. P. *J. Phys. Chem.* **1983**, *87*, 4341–4343.
(55) Hauser, H. *Proc. Natl. Acad. Sci. USA* **1989**, *86*, 5351–5355.

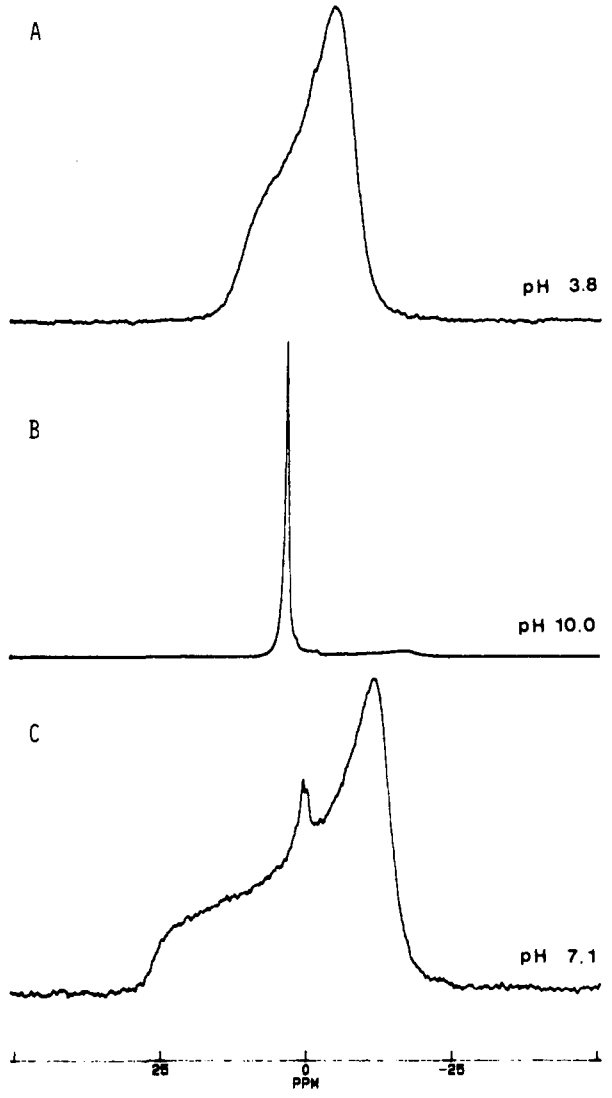

Figure 3. ^{31}P NMR of hydrated **1** during pH jump experiment. A: pH 3.8, hydrated lipid before NaOH addition; sample was a heterogeneous suspension of flocculant solid in water. B: pH 10.0, pH adjusted by addition of 5 N NaOH; sample was homogeneous and a freely flowing fluid. C: pH 7.1, after 6 N HCl neutralization; sample was an opaque, dense gel.

choline (DLPC) on the morphology of **1** is shown in Figures 4A–D. The micrographs are characterized by cross-fractured lamellae with an occasional oblique fracture plane that exposed both the edge and surface of the lamellae (Figure 4A, inset). A peculiar transformation in the bulk properties of the bolalipid dispersions from a transparent fluid to an opaque gel, typically taking place within the first 0.5–2 h after sonication (depending on lipid concentration), is shown on the submicron scale in Figures 4A–C. Immediately after sonication, the appearance of the lipid microstructures is that of "chopped" multilamellae (Figure 4A), as if large multilayer stacks of bolaform lipid have been broken into smaller lamellar arrays during the sonication process. Aging of these samples (and the onset of gelling to a pastelike consistency on the macroscopic scale) caused the stacked layers to delaminate, undulate, and occasionally close to form large unilamellar vesicles (LUVs) and multilamellar vesicles (MLVs) (Figure 4B). When these gels are heated above T_c,[22] the lamellae appear to close, forming exclusively LUVs and MLVs; isolated lamellae are no longer observed (Figure 4C). Sonication of **1** with DLPC (1:2 molar ratio) produced small unilamellar vesicles that displayed both typical and cross-fracturing behavior (Figure 4D and inset). The bifunctional lipids (U-shaped and transmembrane conformations) are believed to be homogeneously mixed with DLPC in the cross-fracturing vesicles; phase separation into DLPC-rich microstructural domains is likely for the vesicles exhibiting typical fracture behavior.

Micrographs of **2** reveal clusters of undulating lamellae with a lower tendency for stacking (Figure 4E) and no observed vesiculation, consistent with the negatively stained TEM results.[22] The degree of layer stacking in **3** appears to exceed that noted for **1** or **2** (compare Figures 4A, E, and F). Although LUVs were occasionally observed in these samples, the bolalipid was predominantly organized as micron-sized arrays of multilayers.

2.2. Cryo-TEM. Additional confirmation of the lamellar morphology assumed by bolalipid dispersions was obtained by cryo-TEM of the same sample used in Figure 4A.[56] Stacked lamellae were observed in these micrographs as well, with visual perspectives both normal to (open arrows in Figure 5) and parallel to the membrane plane (solid arrows in Figure 5) appearing as layered disc-like structures and regularly spaced undulating lines, respectively. Differences in contrast observed in this micrograph are consistent with orthogonal views of the bolaform lipid membrane, i.e., lamellar sheets viewed edge-on produce higher contrast than those viewed side-on. Vesicles of **1** were not seen in any of the cryo-TEM images, although their presence may have been obscured by the abundance of sample regions that were too thick to be imaged.

3. Small-Angle X-ray Scattering (SAXS). Estimates of the membrane thickness from electron microscopy suggested that the bolalipid membrane was approximately 28 Å thick; however, we sought a more precise measurement of the lamellar thickness of **1**. The small-angle diffraction patterns (Figure 6A) show three diffraction orders with relative spacings 1:2:3, confirming the lamellar packing of bolaform lipids below 47 °C. In the wide-angle region, the observed peak at 4.18 $Å^{-1}$ corresponds to the in-plane crystalline packing of the hydrocarbon chains, similar to the L_β or solid phases of phospholipids. At 47.2 °C, both small- and wide-angle patterns undergo dramatic broadening and positional shifts. The wide-angle peak at 4.5 $Å^{-1}$ is characteristic of fluid hydrocarbon chains. The 8-Å reduction in the interlamellar spacing (Figure 6B), the absence of higher-order diffraction peaks, and the large diffraction peak widths for the first-order reflection suggest formation of an isotropic phase rather than an L_α phase above 47 °C.

The interlamellar distance measured at 18.9 °C is in good agreement with the phosphorus–phosphorus separation of **1** determined by CPK models (34 Å) when the membrane-spanning chains are in their all-trans configuration; the small deviation between the experimental and calculated values is most likely due to phosphate-bound water between the lamellae. The T_c measured by SAXS for dry **1** is only 3–4 °C lower than that observed by DSC[22] and Raman spectroscopy (see below) for **1** in excess water. This suggests that the phase transitions observed near 48 °C are melting transitions of the bolaform lipid alkyl chains rather than a process involving membrane swelling, delamination, and water intercalation that would be expected to show a much greater dependence on water content. Similar results have been reported for the monopolar ether lipid 1,2-*O*-dihexadecyl-*sn*-glycerol-3-phosphocholine studied over a wide range of lipid:water ratios.[51,57]

4. Raman Spectroscopy. Raman spectroscopy was chosen to selectively interrogate the molecular structure (e.g., C–H and C–C stretching modes) while passing through the bolalipid phase transition. Figure 7A presents two Raman spectra of hydrated **1** (pH 2.6) obtained above and below the T_c. The bands at 2883 and 2848 cm^{-1} in the 24 °C spectrum are assigned to methylene C–H asymmetric stretching and C–H symmetric modes, respectively, while the small peak at ~2936 cm^{-1} is attributed, in part, to Fermi interaction between an overtone of an asymmetric

(56) Dilution of the sonicated sample of **1** (25 mg/mL) was necessary for practical purposes. It extended the onset of gelation, displayed more favorable spreading properties, and improved sample thinness on the EM grids. Cryo-TEM became impossible if the sample gelled during any stage of sample preparation due to poor spreading or specimens that were excessively thick for imaging.

(57) Laggner, P.; Lohner, K.; Degovics, G.; Müller, K.; Schuster, A. *Chem. Phys. Lipids* **1987**, *44*, 31–60.

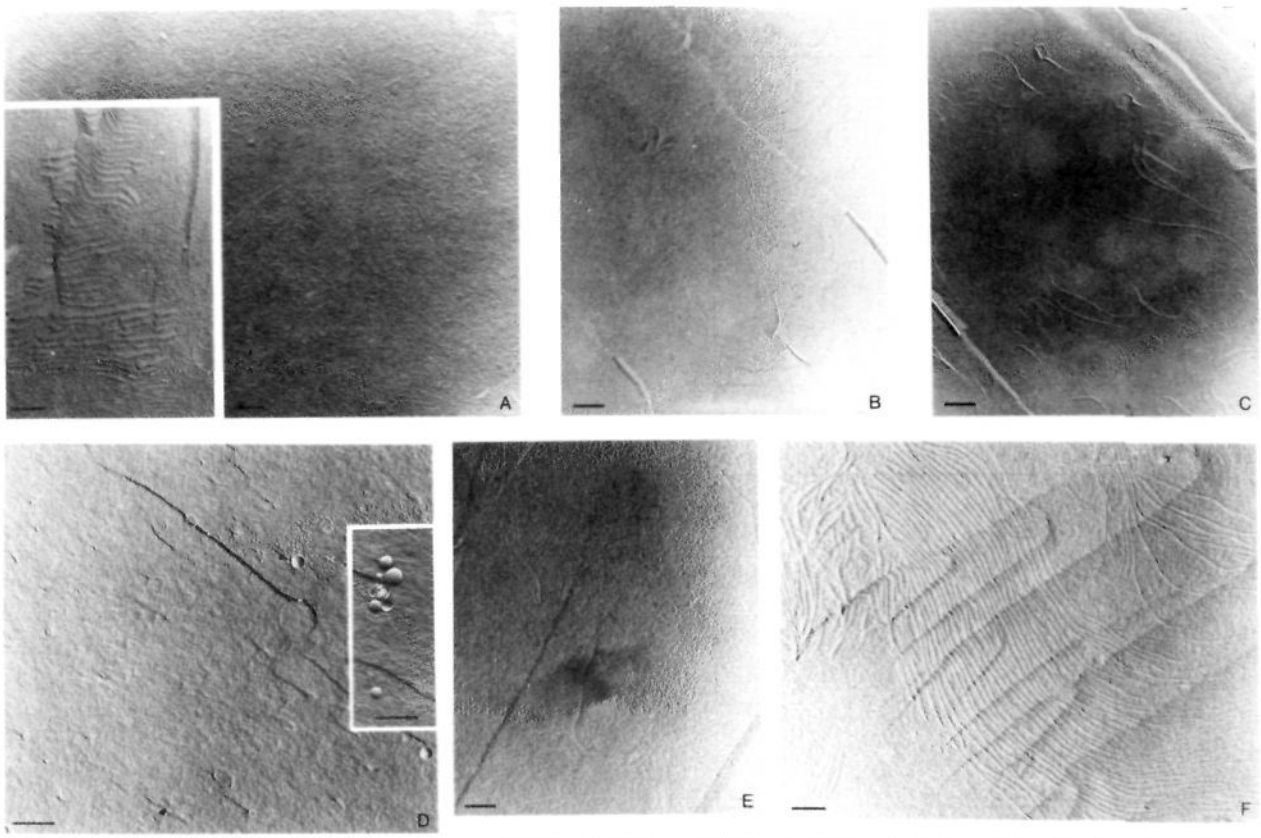

Figure 4. Freeze-fracture TEM of sonicated bolaform amphiphiles. Scale bar = 2000 Å. A: **1**, 25 mg/mL; inset, oblique fracture plane. B: same as Figure 4A, except aged 48 h. C: same as Figure 4B, except heated at 70 °C for 1 h after aging. D: **1** + DLPC (1 mol **1**:2 mol DLPC) immediately after sonication; inset, vesicle cross-fracture plane from the same sample. E: **2**, 5 mg/mL. F: **3**, 40 mg/mL.

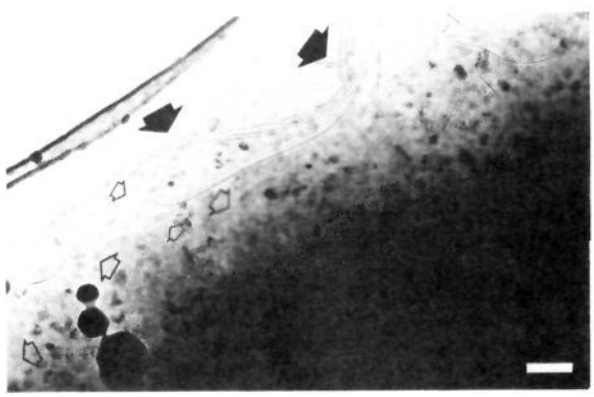

Figure 5. Cryo-TEM of sonicated **1** (12 mg/mL in 40 mM imidazole, pH 6.8; aged 24 h without heat treatment). Scale bar = 2000 Å. Solid arrows: lamellae viewed parallel to membrane plane. Open arrows: lamellae viewed perpendicular to membrane plane.

methyl deformation and a symmetric stretch of the terminal methyl on the decyl chains of **1**.[52,58] Heating of the sample to 60 °C caused the Raman frequencies to broaden and shift to slightly higher frequencies. These temperature-dependent intensity changes in the vibrational modes were plotted according to Levin[58] as the ratio I_{2936}/I_{2883}, or $I_{\text{disordered}}/I_{\text{ordered}}$ (Figure 7B). A dramatic increase in this ratio at 51 °C was noted, corresponding to an abrupt increase in alkyl chain disorder as the stacked monolayer membranes pass from a gel to a liquid crystalline state. The steep onset of this transition is characteristic of multilayer dispersions, in contrast to the more gradual changes noted in $I_{\text{disordered}}/I_{\text{ordered}}$ for vesicular suspensions, and suggests that a more cooperative chain melting process takes place in bolalipid multilayer arrays.

(58) Levin, I. W. In *Advances in Infrared and Raman Spectroscopy*; Clark, R. J. H., Hester, R. E., Eds.; Wiley: Heyden, 1984; Vol. 11, pp 1–48.

Discussion

^{31}P NMR line shapes of hydrated **1** bolaamphiphile (Figures 2A and 3A–C) indicate that this lipid undergoes a transition from an axially symmetric, partially averaged motion to an isotropic motion near 45 °C, consistent with a transition from the lamellar phase to an unknown isotropic phase. The precise nature of this higher temperature phase is uncertain except that the phosphorus environment is undergoing rapid isotropic motional averaging on the NMR timescale due to rapid diffusion and/or tumbling of the lipid aggregate. This would be consistent with delamination of multilamellar stacks (that are "cross-linked" by hydrogen bonding) into isolated lamellae, micellarization, or temperature-induced vesiculation into closed lamellar structures. These interpretations can account for an increase in rapid motion about the P–O monoester and C (glycerol C-3)–O (P–O monoester) bonds due to reduced intermolecular interactions. We favor the latter explanation and attribute the increase in the isotropic signal component with temperature to heat-induced vesiculation, since freeze-fracture TEM shows that closed vesicles form as the suspension is heated beyond its phase transition temperature (Figures 4A–C). This effect also accounts for the isotropic phosphorus component observed at temperatures below 20 °C (Figures 2A and C) since these spectra were recorded immediately *after* the heating cycle (i.e., before the sample was fully equilibrated).

Further insight into the molecular motions of these lipids can be derived by analysis of the temperature-dependent CSAs. Variable temperature ^{31}P NMR powder patterns for **1**, **2**, and **4** exhibit a negative sign for the chemical shift anisotropy characteristic of the lamellar phase. The CSA of **4** is reduced by a factor of 2 relative to **1** over the entire temperature range (Figure 8). This trend is consistent with the shorter alkyl chain length of **4** and implies a significantly reduced orientational ordering. It is interesting to note that **2** shows a similar reduction in CSA

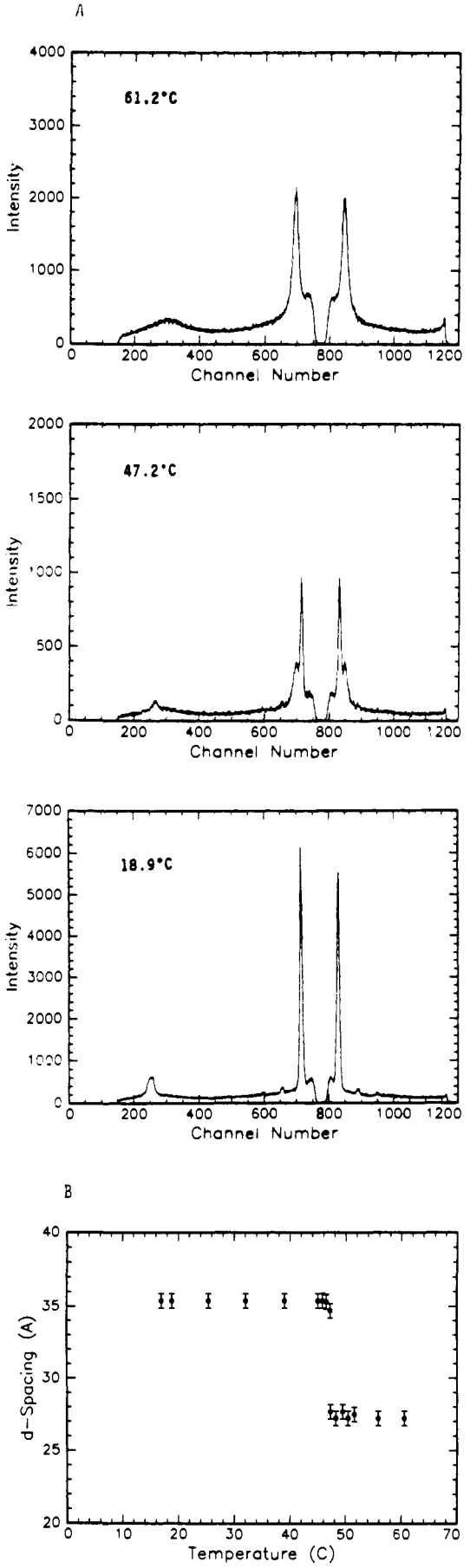

Figure 6. Small-angle X-ray scattering analysis of dry **1**. System calibration was performed using cadmium stearate. A: temperature-dependent intensity vs channel number. B: d-spacing vs temperature.

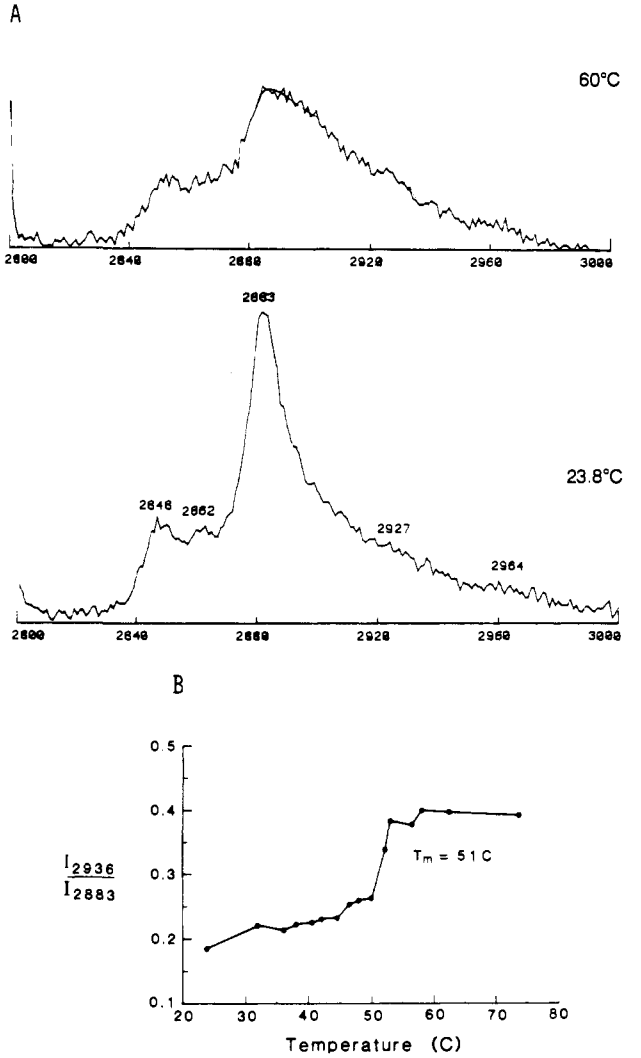

Figure 7. Temperature-dependent Raman spectroscopy of **1** at pH 2.6. A: Raman spectra at 60 °C (upper) and 23.8 °C (lower). B: intensity ratio of disordered/ordered C–H vibrations as a function of temperature.

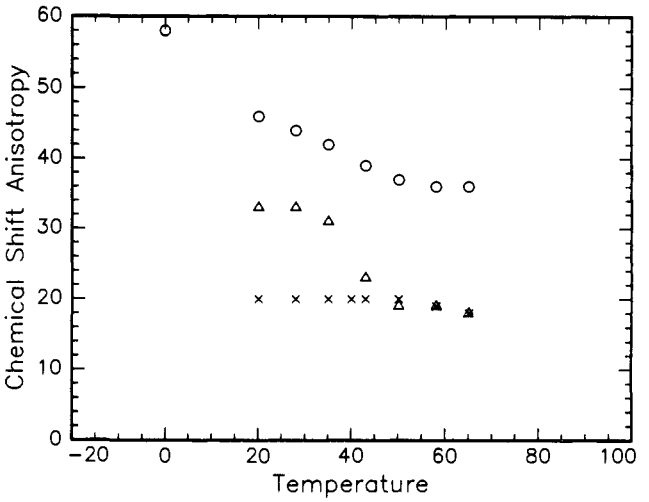

Figure 8. Change in chemical shift anisotropy ($\Delta\sigma$) as a function of temperature for **1** (○), **2** (△), and **4** (×).

compared with **1** even though the membrane-spanning alkyl chain lengths are the same. Reorientation of the headgroup around the membrane-spanning segment may account for the observed reduction in CSA. Using a symmetry axis collinear with the membrane-spanning alkyl chain and a 35.5° effective tilt angle of the C-3 glycerol phosphate headgroup segment with respect

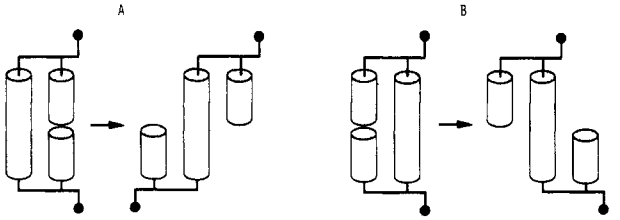

Figure 9. Rotational diffusion model for coupled alkyl chain and phosphorus atom motions for **1** (A) and **2** (B).

to the symmetry axis, a 2-fold reduction in CSA, with no change in its sign, is predicted in accordance with experimental results. The corresponding internal rotation in **1** is less likely since it would lead to unfavorable molecular conformations, inefficient packing (see Figure 9), and higher CSAs than have been observed in our experiments. Bolalipid **3** differs from the rest since it has two distinctly different phosphorus sites. The site symmetry of the linear phosphate monoester resembles that found in **1**; however, the other phosphorus site is located within a five-membered ring. Significantly more motional averaging is possible for the cyclic phosphodiester due to multiple bond reorientations within the membrane-spanning segment. Therefore, the spectra in Figure 2C contain a superposition of a broad monoester phosphate component and a narrow cyclic phosphodiester signal with a chemical shift anisotropy comparable to that determined for **1**. Bolalipids **1** and **3** also show significant decreases in CSA above room temperature analogous to the CSA decreases observed for the L_β–P_β and P_β–L_α phase transitions in phospholipids.[59] The decrease in CSA with increasing temperature may be associated with pretransitional reductions in the orientational ordering, consistent with the Raman data.

U-shaped conformations at the air–water interface have been reported for bolalipid **1**[22] and naturally occurring thermacidophilic archaebacterial lipids such as glycerol dialkyl nonitol tetraether (GDNT) at low surface pressures.[12] This conformation makes a relatively minor contribution to the predominantly transmembrane bolaform lipid conformation; however, since (1) the lamellar distance for **1** observed by SAXS corresponds to the spacing that would be expected for an all-trans configuration of the aliphatic segments and (2) the ratio $I_{\text{disordered}}/I_{\text{ordered}}$ for **1** is low relative to that for phosphatidylcholine multilayers in the gel phase.[58,60] This suggests that the bolaamphiphiles exist in a predominantly anti chain conformation with very little contribution to the gauche vibrational modes that would be expected if large proportions of the lipid were in a U-shaped conformation. In principle, a bilayer structure composed of U-configured bolaamphiphiles might yield similar SAXS d-spacings; however, we discount this possibility for several reasons. A U-shaped lipid conformation would require intercalation of opposing monolayers in the case of **3** and would be expected to produce higher $I_{\text{disordered}}/I_{\text{ordered}}$ ratios as a result of more poorly packed membranes. The observed aging or hydration-induced delamination (Figure 4B) of stacked, intercalated membranes also would not be expected since this would expose the intercalated alkyl chains to bulk water and would require concomitant delamination and chain melting processes.[61] Major contributions from a U-shaped bolalipid conformation should also lead to freeze-fracture behavior of **1**–**3** (**4** not analyzed by freeze-fracture TEM), showing catastrophic failure along the midplane of the bilayer as is typical for bilayer membranes.[46] This is, in fact, not the case since *exclusively* cross-fractured membranes are observed for all pure bolaform amphiphile dispersions.

The absence of stain-induced artifacts in our earlier TEM work is clear since negative staining, freeze-fracture, and cryo-TEM methods all depict the bolaform lipid membranes as multilamellar below T_c. Extensive freeze-fracture experiments with **1** have shown that the multilayer organization is transformed by sonication, aging, and heating. Our model for these processes (Figure 10) involves multilamellar fracturing by sonication to produce smaller arrays of stacked layers, interpenetration of water between the stacks upon aging to give isolated, freely undulating lamellar discs,[62] closing of the lamellae to form MLVs and LUVs above the phase transition temperature or at high pH, and reformation of the multilamellar network upon drying. (A similar, temperature-induced transformation from multilamellar rods to vesicles has been reported for the glycolipid 1,2-*O*-ditetradecyl-3-*O*-β-D-galactosyl-*sn*-glycerol[63] that also has strongly hydrogen-bonded headgroups. A more general model for vesicle formation by charged and uncharged lipids has also been reported.[64]) This model also suggests a molecular basis for gelation wherein hydration and swelling of the membranes creates a network of undulating layers rigidified by "cross-linking", via hydrogen bonds or cation bridges between the phosphate headgroups of the bifunctional lipids in neighboring layers, to form a three-dimensional web of contact points throughout the gel. Cation bridging between negatively charged phosphate headgroups would also account for the increase in chemical shift anisotropy at pH 7.1 (Figure 3C) relative to that observed at pH 3.8 (Figure 3C) where the phosphate headgroups are more fully protonated and engaged in weaker hydrogen bonding, resulting in more rapid axial diffusion and narrower line shapes.

Self-consistency in the bolalipid phase transition temperatures determined by DSC (49 °C)[22] and Raman spectroscopy (51 °C) and the observed decrease in the ^{31}P NMR chemical shift anisotropies over the same temperature range create a detailed picture of how alkyl chain packing and phosphate headgroup motion change as a function of temperature and suggest that alkyl chain packing may be crystal-like (i.e., predominantly anti conformations) even in aqueous dispersions since the measured melting transitions are near that of the dry lipid. These transitions are also in the range of values reported for the ester-linked zwitterionic lipid 1,2-dioctadecanoyl-*sn*-glycero-3-phosphocholine (T_c = 53.5 °C)[58] and the ether-linked lipid 1,2-*O*-dihexadecyl-*rac*-glycerophosphate (T_c = 50 °C).[65] We infer from these data that the phase transitions of new bolalipid lamellar phases might be predictable, to a first approximation, on the basis of the knowledge of the T_cs of monopolar lipids of similar chain length.

Considerations of supramolecular organization within bolaform lipid lamellae lead to interesting chain packing problems if packing is assumed to be analogous to that adopted in the crystal structure of 1,2-dilauroyl-*sn*-glycero-3-phosphate (DLPA), where the bilayer thickness is 35.7 Å with a molecular axis tilt of 31° and a molecular area of 43.3 Å^2/molecule.[66,67] The membrane thickness (35.5 Å) and molecular area[68] measured by SAXS in our bolalipid sample is in good agreement with the DLPA values. Examination of molecular models would suggest that either the lipid has no tilt angle and the glycerol interfacial segment runs parallel to the membrane plane or the two glycerols of a single bolalipid are antiparallel within the lamellae allowing for a molecular tilt by intercalation of the shorter chains (Figure 11); however, the la-

(59) Trahms, L.; Klabe, W. D. *Mol. Cryst. Liq. Cryst.* **1985**, *123*, 333–345.
(60) Indeed, I_{2883}/I_{2936} for **1** above T_c is comparable with that observed for the gel phase of phosphatidylcholines, suggesting a greater degree of orientational ordering for bolalipids in their higher temperature phases ($I_{2883}/I_{2936} \simeq 0.4$ for **1** at 60 °C) than is found for phospholipids below T_c (I_{2883}/I_{2936} for DPPC ≈ 0.4 in L_β-phase at 27 °C).
(61) This might be possible if the shorter bolaamphiphile alkyl segments (i.e., the C_8 or C_{10} chains) from one lamella were intercalated into neighboring lamellae such that delamination of the multilayers resulted in abrupt relocation of the "guest" alkyl chains to the "host" membrane resulting in disordered, poorly packed lipids.
(62) Disc-like micelles have recently been reported in amphotericin B preparations: Lasic, D. D. *Nature* **1992**, *355*, 279–280.
(63) Kuttenreich, H.; Hinz, H. J.; Inczedy-Marcsek, M.; Koinova, R.; Tenchov, B.; Laggner, P. *Chem. Phys. Lipids* **1988**, *47*, 245–260.
(64) Lasic, D. D. *Biochem. J.* **1988**, *256*, 1–11.
(65) Vogel, H.; Jahnig, F. *Chem. Phys. Lipids* **1981**, *29*, 83–101.
(66) Marsh, D. *Handbook of Lipid Bilayers*; CRC Press: Boca Raton, FL, 1990; p 87.
(67) Hauser, H.; Pascher, I.; Sundell, S. *Biochemistry* **1988**, *27*, 9166–9174.
(68) The molecular cross-sectional area was determined by SAXS using the formula $S_a = M_a/(N_A \rho_a d_a)$, where M_a, ρ_a, and d_a are the lipid molecular weight (902 g/mol), lipid density (≃1), and the lamellar thickness (35.5 Å), respectively.

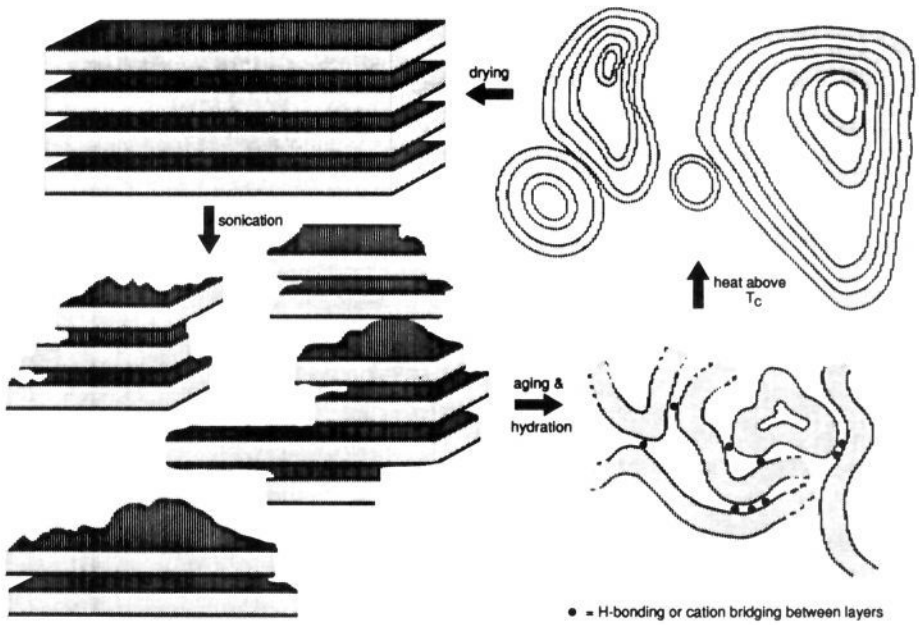

Figure 10. Proposed model for delamination and vesiculation of bolaform lipids.

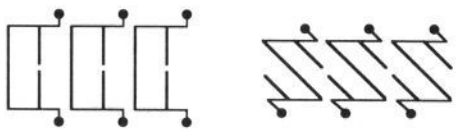

Figure 11. Perpendicular and tilted packing models for bolaform amphiphile lipid membranes.

mellar thickness of the latter conformation is inconsistent with the SAXS data.

Cyclic[69] and monophosphate[70] esters of glycerophytanyl ethers have been recently reported as constituents of halophilic archaebacterial membranes. Therefore, our structural investigations on the synthetic ether-linked bolaform lipids **1–4** may provide additional insight into the properties of the naturally occurring materials after which they were patterned. Indeed, the similarity between our observations and those obtained with hydrolyzed, naturally occurring bolalipids with respect to their tendency to form "filamentlike structures" that "seem to break, resulting in smaller aggregates of polydisperse sizes" forming "wrinkled-like liposomes ... in addition to onion like structures"[71] suggests that alkyl chain physical state and interlayer interactions may dictate the supramolecular properties of long-chain bifunctional lipid lamellae in general.

Conclusions

The results of our experiments suggest that the difficulties encountered in dispersing long-chain, self-assembling bolaform lipids beyond multilamellar stacks[22,24] arise from improved chain packing and interlamellar "cross-linking" (via hydrogen bonding) that are a direct consequence of the bifunctional nature of the amphiphiles. Vesiculation occurs more readily in Führhop's dodecyl-based bolas[16,17] due to greater chain disorder and reduced hydrophobic interactions between the shorter C_{12} chains[72] leading to higher water solubilities and critical micelle concentrations. Highly ordered alkyl chains indicated by our Raman results suggest that the bolaamphiphiles adopt primarily a "membrane-spanning" geometry that places headgroups on opposing lamellar interfaces with minimal contributions arising from a U-shaped configuration. These data support similar conclusions made regarding bolalipid structuring on the basis of chemical reactivity[20] and contact shifts observed in mixed phosphatidylcholine–archaebacterial lipid vesicles[71] and hint at the relevance of these synthetic materials to their naturally occurring, archaebacterial counterparts.

Insights gained into the structure/property relationships of ether-linked, bolaform amphiphile behaviors are now being used to design and prepare new ultrathin membrane materials capable of optimizing transmembrane charge separation processes.

Acknowledgment. Financial support by the U.S. Department of Energy, Office of Basic Energy Sciences (Grant No. DE-FG06-88ER13963) is gratefully acknowledged. We also thank Professor Thomas M. Loehr for providing access to Raman instrumentation and Professor Joseph Zazadsinski for helpful discussions.

Registry No. 1, 138355-12-1; **2**, 138355-14-3; **3**, 138355-13-2; **4**, 138355-15-4; DLPC, 18194-25-7.

(69) Lanzotti, V.; Nicolaus, B.; Trincone, A.; De Rosa, M.; Grant, W. D.; Gambacorta, A. *Biochim. Biophys. Acta* **1989**, *1001*, 31–34.
(70) Lanzotti, V.; Nicolaus, B.; Trincone, A.; De Rosa, M.; Grant, W. D.; Gambacorta, A. *Biochim. Biophys. Acta* **1989**, *1002*, 398–400.
(71) Mirghani, Z.; Bertoia, D.; Gliozzi, A.; De Rosa, M.; Gambacorta, A. *Chem. Phys. Lipids* **1990**, *55*, 85–96.

(72) The sulfone and sulfonic acid headgroups of these materials have greatly reduced hydrogen-bonding opportunities relative to phosphate monoesters and cyclic diesters **1–4**.